A multi-step cold plasma process for fine tuning of polymer nanostructuring

Andrii Zaitsev, Fabienne Poncin-Epaillard, Ana Lacoste, Adi Kassiba, Dominique Debarnot

A multi-step cold plasma process for fine tuning of polymer nanostructuring

Andrii Zaitsev[1], Fabienne Poncin-Epaillard[1], Ana Lacoste[2], Adi Kassiba[1], Dominique Debarnot[1]*

[1]Institut des Molécules et Matériaux du Mans (IMMM) - UMR 6283 CNRS, Le Mans Université, Avenue Olivier Messiaen, 72085 Le Mans Cedex 9, France

[2]LPSC, Université Grenoble-Alpes, CNRS/IN2P3, 53 rue des Martyrs, 38026 Grenoble, France

[*] Corresponding author: Dominique.Debarnot@univ-lemans.fr

Progress Org. Coat., **128**, 112-119 (2019)

Abstract

The innovative plasma process, developed in this study for highly structured surfaces, consists to gradually decrease the input power during deposition in order to form polymer nuclei while preserving monomer structure. In such a process, the local heating of the surface at the starting high discharge power seems to control the lateral migration of deposited species on the surface. Therefore, the objective of the current work is to control the substrate surface heating in order to achieve the morphology of the polymer (polyaniline), namely the dimensions of the nanostructures. This requires studying the high-power step through the value of the power, its duration and the number of steps. All these parameters are herein examined on both the chemical and morphological structure of the plasma-polymer. The power variation is shown to have a double effect. Indeed, high value at the first step is required for increasing the surface temperature and allowing nuclei formation but a too high power induces a degradation of the formed nanodots. Moreover, the

sensitivity to ammonia gas of such textured polyaniline films is examined and compared to smooth polymer layers.

Keywords: nanostructures; polyaniline; cold plasma; multi-step process; gas detection.

1. Introduction

One-dimensional polymers' structures have attracted a growing interest recently due to their interesting properties such as a high shape factor. In particular, this property allows improving characteristics of sensors such as their sensitivity. For this specific application, doped polyaniline is a good candidate due to its sensitivity at room temperature and its selectivity to ammonia gas [1-3]. Conventional polyaniline contains two types of chain units (Figure 1) arranged randomly through the polymer chain.

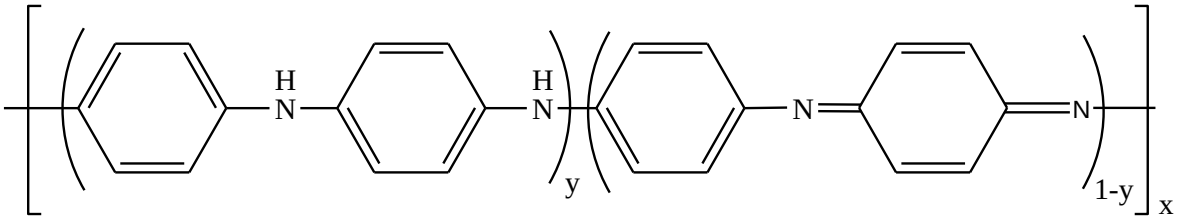

Figure 1. Chemical composition of polyaniline. y denotes the oxidation degree of the polymer and x, the chain length.

While chemical and electrochemical syntheses of one-dimensional structures were widely studied [4-13], they require some additional chemicals such as oxidants and acids as well as post-synthesis steps of filtration and drying. The obtained polymer is usually a powder, so further treatment is necessary for shaping the material before its integration into a device. Another approach consists in using different types of templates such as anodic alumina membranes, carbon

nanotubes, TiO_2 nanorods,… [14-20] This is a promising path that does not need any additional products but pre-formed surfaces are required as well as a post-synthesis step for the template dissolution.

The elaboration of one-dimensional structures by plasma polymerization, despite its advantages (one step, direct synthesis and deposition of the polymer onto the support), is not well developed: most of synthesized films described in literature are smooth [21-25]. However, some groups have reported the formation of nanostructured plasma polymerized (pp) films. In the work of Kumar *et al.* [26,27], pulsed plasma polymerization of aniline (ANI) was conducted with pulsed injection of the monomer that led to nanofibrous films for NO_2 sensing. Michelmore *et al.* [28] have demonstrated that the chemical nature of amine-containing monomers (allylamine or heptylamine) has a significant impact on the nanomorphology of the films in the early stages of plasma deposition. With heptylamine, island-like growth is initially observed whereas coatings grown from allylamine are smooth from the very earliest stages. The latter result has been confirmed by Choukourov [29] that showed that even very thin pp-allylamine films (< 10 nm) are continuous. The works of Hegemann *et al.* [30] have shown the formation of nanopores in amine-containing hydrocarbon films at moderate energetic conditions with a high accessibility of the amino-functional groups. By using fluorinated precursors [31,32], Favia *et al.* have obtained different micro/nanostructures (ribbons and petals) while working in modulated r.f. plasma. In the same line, the works of Brioude *et al.* [33,34] on the plasma polymerization of maleic anhydride allowed obtaining spherical or branched structures in pulsed excitation mode. These two last groups have ascribed the formation of the structures to the competition between rate of deposition and rate of diffusion of active species.

The structures elaborated in these studies are not aligned perpendicular to the surface. It can be explained by the absence of specific growth sites during plasma polymerization contrary to

conventional polymerization in solution (oligomers) [13] or carbon nanotubes growth (metallic particles) [35-38]. Some other studies describe plasma etching of the surfaces ("top-down" method) [39-41]. The major drawback of this method is the alteration of the polymer chemical structure that limits the range of applications of such a structure.

Our team has recently developed a novel plasma polymerization process yielding highly structured surfaces without using any template [42]. It consists in varying the input power during deposition, starting with a high value in order to form polymer nuclei followed by a low value to preserve the monomer structure. We made the hypothesis that this structuring is due to the local heating of the surface at high discharge power allowing lateral migration of deposited species and formation of droplets onto the surface. The objective of this work is to control the substrate surface heating in order to control the morphology of the polymer, namely the dimensions of the nanostructures. This requires studying the high-power step through the value of the input power, its duration and the number of steps. All these parameters are herein examined on both the chemical and morphological structure of the plasma polymerized aniline films.

Moreover, in order to illustrate the importance of surface structuring for some applications, our textured pp-ANI films are tested for their sensitivity to ammonia gas. When ammonia gas interacts with doped pp-ANI layer, the doping state of the plasma polymer changes [3]. Consequently, electrical and optical properties of pp-ANI are modified. In this work, the optical properties of the films are measured through a variation in absorbance.

2. Experimental

2.1. Substrate preparation

Polyaniline films were deposited onto clean silicon wafers (100). In order to remove the surface contamination, wafers were cleaned with acetone and ethanol in ultrasonic bath (10 min) and rinsed

with deionized water. Finally, the wafers were immersed into boiling piranha solution (H_2SO_4:H_2O_2=3:1), then rinsed with deionized water and dried with compressed air. The wafers were exposed to UV light for 10 min prior to use.

2.2. Polyaniline synthesis

A plasma reactor with distributed microwave sources (Boréal Plasmas 7050) was used and has been described in a previous publication [42]. Twelve microwave sources (electronic cyclotronic resonance (ECR) applicators) are distributed along the circumference. This configuration allows working at low precursor pressure (down to 0.01 Pa) leading to a high plasma homogeneity and scalability.

The system was pumped to a base pressure of 5×10^{-3} Pa using a turbomolecular pump (Adixen ATH300Ci) backed up by a dry pump (Adixen ACP28G). The pressure in the chamber was measured using a Pirani-cold cathode combined gauge (Pfeiffer PKR251). Liquid aniline (Sigma-Aldrich, *ReagentPlus*®, 99%) was in a glass tube which was connected to the vacuum through the upper flange of the plasma chamber. This tube was maintained at 40°C by hot water. The working pressure of aniline vapor was fixed at 0.2 Pa and was measured by a capacitive gauge (Pfeiffer CCR364). The calculated flow rate (as measured by weighing the tube with aniline before and after deposition) was 1.6 g/h. The sample was placed on the water cooled substrate-holder situated in the post-discharge zone, at the bottom center of the chamber. In the post-discharge zone, the functional groups of the monomer were better retained than in the glow discharge. The plasma was generated using a microwave generator (Sairem GMP20KED 2.45 GHz) and the reflected power was minimized separately for every applicator. The deposition time was varied between 1 and 10 min. The input power was varied from 60 W (minimum restricted by microwave generator) to 480 W.

2.3. Surface temperature measurements

The substrate temperature was determined thanks to Thermax indicators purchased from Manutan (Pontoise, France) with a temperature detection range going from 37°C to 65°C. Thermax indicators are self-adhesive labels composed of a series of temperature-sensitive elements. These elements irreversibly turn from white to black when the corresponding temperature is attained. The indicator keeps its black color even if the subsequent temperature decreases. The Thermax indicators are sensitive to the temperature of the surface on which they are applied, rather than that of the atmosphere. In our study, the tape was affixed on a silicon wafer which was then placed on the substrate holder. The temperature was *in-situ* read through the window of the plasma reactor during deposition.

2.4. Atomic force microscopy measurements

AFM was performed using Bruker Innova atomic force microscope in tapping mode on the films deposited onto silicon substrates. The cantilever (antimony-doped silicon, Bruker) had a typical stiffness coefficient of 40 N/m and a resonant frequency near 300 kHz. Scan region was fixed at 5x5 μm, scan frequency at 0.75 Hz with 512 samples and 512 lines. Raw data was treated with Gwyddion software (mean plane subtraction, root mean square roughness (R_q) calculation and statistics on grains).

2.5. FT-IR measurements

The FT-IR spectroscopy was performed on a Bruker IFS66 spectrometer (Globar source, 32 scans, DTGS detector, resolution 2 cm^{-1}) in transmission mode on pp-ANI films deposited directly onto potassium bromide (KBr, Sigma-Aldrich, FT-IR grade 99.99%) pellets. In order to prepare

KBr pellets, 100 mg of KBr were introduced into stainless steel form (diameter 10 mm, Eurolabo) and then pressed under 12 tons for 3 min. A pure KBr pellet was used as reference.

Transmittance spectra were treated with Opus software for baseline correction (polynomial) and CO_2/H_2O compensation and also normalized with respect to the thickness.

The amount of C-H and C=C bonds in pp-ANI films elaborated at different discharge powers has been determined by area measurement of the bands centered at (i) 2930 cm^{-1} (saturated C-H stretch) and 3030 cm^{-1} (unsaturated C-H stretch) for C-H bonds; (ii) 1500 cm^{-1} (aromatic C=C stretch) and 1600 cm^{-1} (aromatic and aliphatic C=C stretch) for C=C bonds [42].

2.6. XPS measurements

For the XPS measurements, the films were deposited onto Si/SiO_2 wafers (Siltronix, France) and then analyzed using Kratos Axis Nova instrument. The photoemission was excited by a monochromatic Al Kα beam. The narrow scans of the C1s and N1s were acquired with steps of 0.1 eV and a pass energy of 20 eV. The spectra were taken with the electron emission angle at 90° relative to the sample surface, yielding a maximum sampling depth around 10 nm due to the mean free path of the electrons. Calibration was conducted on the C 1s peak of the C–C, C–H and C=C bonds at 285 eV. The position and scale in energy were regularly checked by using reference samples of gold, copper and silver so that the error on the position of the peaks is ±0.1 eV. The curve fitting was performed using CasaXPS software (Casa Software Ltd.). The peak shape was chosen with Gaussian (70%) / Lorentzian (30%) curve fitting. The elemental quantification accuracy was 5%.

The high resolution C1s XPS spectra of all pp-ANI films have been decomposed in four components at (i) 285 eV attributed to C-C, C-H, C=C; (ii) 285.9 eV assigned to C-N, C-O; (iii) 286.8 eV corresponding to C≡N and (iv) 288.1 eV due to O=C-N, C=O and N-C-O.

2.7. Thickness measurements

The thickness of the pp-ANI films deposited onto silicon wafers was measured thanks to a mechanical profilometer (Dektak 8, Veeco). The principle of this technique was to measure the height of a step corresponding to the thickness of the polymer layer. In order to create this step, a mask was placed on a part of the substrate before deposition and was removed once the deposition was finished. Then, the tip of the profilometer was scanned over the sample surface along a straight line.

The film thickness value for a sample represents the average of six different measurements.

2.8. Electron Spin Resonance (ESR) measurement

ESR investigations were carried on BRUKER EMX spectrometer equipped with X-band microwave bridge (9.5 GHz). For an ESR experiment, a suprasil quartz tube containing the pp-ANI film deposited onto a polyvinylchloride (PVC) substrate was placed in the microwave resonant cavity and was submitted to a static magnetic field swept in the range 3000 - 4000 Gauss. The recorded ESR spectrum was adjusted by usual powder-like commercial software Bruker Simfonia for paramagnetic species with spin S=1/2. The spectral parameters of ESR spectrum (line position, width, intensity) were estimated to assign the nature of paramagnetic radicals and their interactions with their environment. The absolute concentration of radicals was estimated by double integration of the ESR signal and comparison with the signal from copper sulfate standard sample.

2.9. Optical sensing system

The optical sensor is made of doped pp-ANI film deposited onto glass substrate as described above, and placed into the measuring chamber. The doping method consisted in introducing pp-ANI layer into a chamber saturated with iodine (I_2, Aldrich) vapors during 48 h. pp-ANI doping allows creating radical cations (or polarons, $N^{+\bullet}$) which are the ammonia absorption sites. The optical ammonia gas sensing system has already been described in a previous publication [3]. It consists of a Cary 100 spectrophotometer in which the sealed measuring chamber has been inserted, a gas dilution system with flowmeters and a computer for data collection and analysis. At the beginning of the experiment, the zero point of the spectrometer was carried out without the pp-ANI sensor. Nitrogen gas (99.99%, Air Liquide) was used as dilution gas. The flows of ammonia and nitrogen gases were precisely controlled by two flowmeters, which were plugged in a mass flow controller (MFC). The concentration of NH_3 gas in the measuring chamber was varied by mixing different flows of NH_3 gas and 500 sccm of N_2 gas. The concentration of NH_3 (ppm) was defined as the ratio of the flow rate of NH_3 gas to the total flow rate of NH_3 and N_2 gases. In this work, the ammonia concentration was fixed at 4618 ppm. After inserting the pp-ANI sensor inside the measuring chamber, a certain amount of dried ammonia gas, diluted in nitrogen gas, was introduced into the measuring chamber. The interaction between NH_3 gas and the pp-ANI film leads to optical absorbance variation of pp-ANI. When the optical absorbance variation tends to a constant value depending on time, the NH_3 gas introduction was turned off and stream of pure N_2 gas was passed through the sensor to purge completely the NH_3 molecules in the measuring chamber and to regenerate the polyaniline sensor.

Sensitivity (S) was calculated as $(A-A_0)/A_0$ ratio, where A_0 is the initial optical absorbance of the sensor under N_2 and A the absorbance of the sensor when exposed to ammonia gas. The wavelength

of the light source used in this work was fixed at 430 nm. All experiments were performed at room temperature.

3. Results and Discussion

The first part of this section is dedicated to the two-step process where a high power is applied for a short time before low-power deposition that creates a nanostructured surface with preservation of the monomer entity. The second part deals with the three-step process where the applied power is reduced stepwise for a better control over the structuring process.

3.1. Two-step process

Herein, we study the influence of the power and the duration of the first step on the overall morphology. The films are deposited following the two-step process where the power of the first step is varied from 240 W to 420 W and its duration from 1 min to 3 min. The power and duration of the last step are left unchanged for every experience, at 60 W and 26 min respectively.

3.1.1. Chemical structure

The chemical structure of the pp-ANI film deposited thanks to the two-step process (at 240 W during 1 min, then at 60 W during 26 min) is investigated by means of FT-IR and X-ray photoelectron spectroscopies. The first technique allows the analysis of the full film thickness whereas thanks to the second one, only the extreme surface (around 10 nm) is analyzed. The results are compared with those obtained for films synthesized in one step at 240 W or at 60 W (Figure 2).

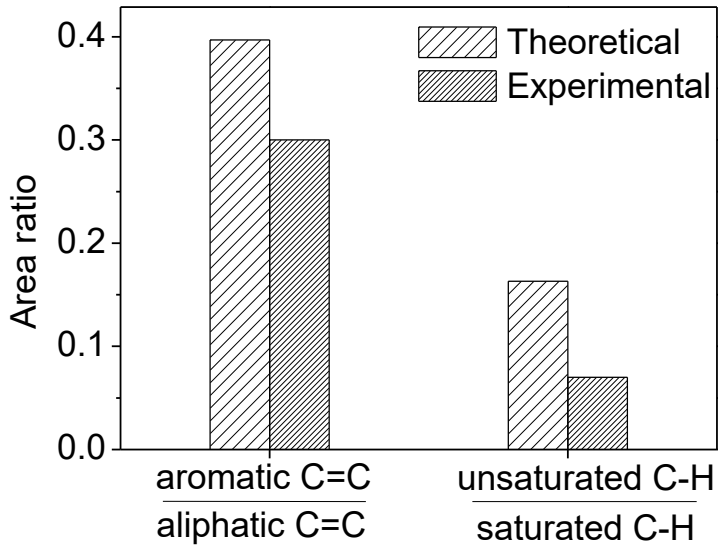

(a)

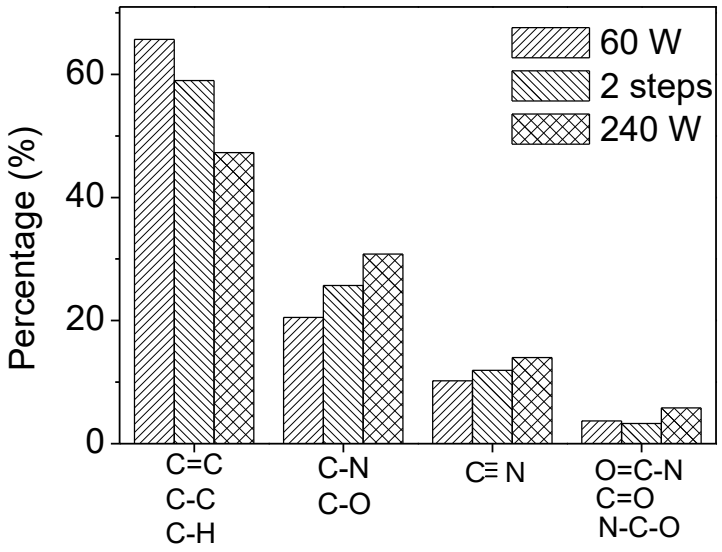

(b)

Figure 2. Chemical structure of pp-ANI films deposited by the two-step process (1 min-240 W→26 min-60 W) or by the one-step one at 240 W or 60 W and analyzed by a) FT-IR spectroscopy and b) XPS.

As regards with the theoretical ratio in Figure 2a, each band area (aromatic and aliphatic C=C, unsaturated and saturated C-H) is the sum of FT-IR band areas of the film synthesized in one step

at 240 W for 1 min (plasma conditions of the first step in the two-step process) and at 60 W for 26 min (plasma conditions of the second step in the two-step process). Figure 2a shows that the experimental values are lower than predicted ones. This result reveals an interaction between the two layers that leads to the degradation of the upper one. This phenomenon is characterized by a loss of functional groups (the aromatic rings) by π-bond scission and aromatic ring opening. Figure 2b supports this observation. It shows the proportion of each of the C1s components (see §2.6) when pp-ANI film is synthesized either by the two-step process or by the single-step one. XPS analysis allows for investigation of a maximum depth around 10 nm. Thus, in the two-step process, no contribution of the bottom layer should be visible if it does not interact with the upper one whose thickness is nearly 260 nm. However, we do observe a difference between relative percentages of chemical bonds determined by XPS for pp-ANI deposited at 60 W or by the two-step process. In fact, the chemical composition of the pp-ANI bilayer is comprised between that of the films elaborated at 240 W or at 60 W. Such a behaviour could be due to the diffusion of the radicals, formed in a larger number at high power (240 W), from the bottom layer to the top one. In order to identify and quantify these radicals, ESR measurements have been applied on pp-ANI films elaborated by the one-step process. When exposed to air, the plasma-polymers develop a large concentration of paramagnetic radicals (Figure 3a – solid line).

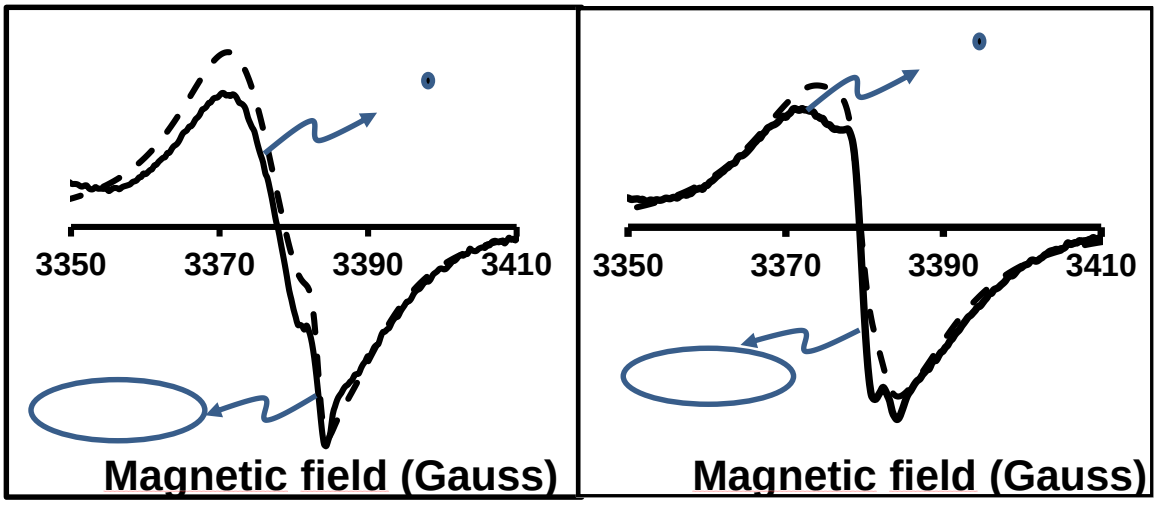

(a) (b)

Figure 3. Experimental (solid line) and simulated (dashed lines) ESR spectra on a small range of the magnetic field leading to a better resolution (a) under air or (b) under argon. (*P* = 120 W, deposition time = 20 min)

The main interaction involved for such paramagnetic radicals is represented by the Zeeman Hamiltonian $\hat{H} = \beta.\vec{B}.\tilde{g}.\vec{S}$ where β represents the Bohr magnetron, B the static magnetic field, $\tilde{g}$ the Landé tensor and S the radical electronic spin. A simple procedure of a crude simulation leads to a characteristic axial g-tensor with components as $g_{\perp} = 2.013 \, and \, g_{//} = 2.008$ (Figure 3a - dashed lines). The obtained values are consistent with those related to oxygen radicals in agreement with a former report [43]. Indeed, just after deposition, the pp-ANI film interacts with the oxygen in the air leading to peroxide radicals which are formed on the reaction sites of pp-ANI surface. In addition to the ESR signal of oxygen radicals, a narrow ESR line is well resolved on the spectra. The corresponding spectral parameters consist in a small line width (2.2 Gauss) and an average <g> equals to 2.006. A possible origin of this signal could be related to the existence of free charges in irradiated polyaniline creating mobile polarons with respect to their motional narrowed

resonance line [44]. Therefore, the ESR spectrum under air is composed of the $O_2^{\bullet}$ signal with high intensity superimposed on that of polarons radicals with weak intensity. The shape of the ESR signal is different when pp-ANI is kept under Ar (Figure 3b). In this case, just after the plasma polymerization, the pp-ANI film is inserted into a quartz tube which is rapidly closed under an argon atmosphere. The ESR spectrum consists in a contribution from $O_2^{\bullet}$ radicals that have reacted with polyaniline and a second one, related to the polarons' signal whose intensity is higher compared to air. Indeed, under Ar, only a small fraction of polarons reacts with oxygen to form peroxide radicals.

The concentration of these radicals is determined from the integrated intensity of the ESR signal. Figure 4 presents the radicals' concentration in pp-ANI films elaborated in one step at different input powers or deposition times. The concentration in radicals remains almost constant until 120 W (deposition time = 20 min) or 20 min (input power = 120 W) and then strongly rises. These radicals could produce different reactions, chain reorganization or scission in the upper layer (60 W) altering its chemical structure. Moreover, the radicals can create bridges between polymer chains increasing the polymer cross-linking.

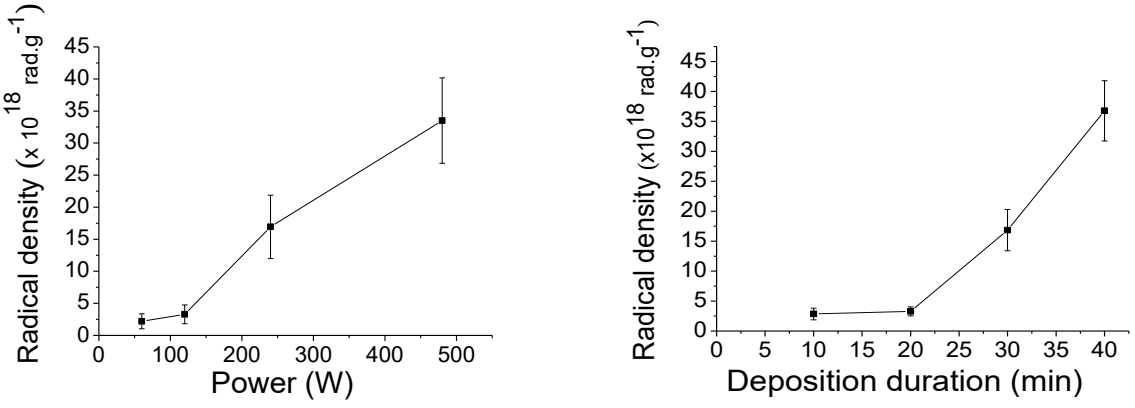

(a) (b)

Figure 4. Evolution of radicals concentration of pp-ANI layers with (a) the input power (deposition time = 20 min) and (b) the deposition time (P = 120 W).

3.1.2. Morphological structure

The morphological structure of the polyaniline films elaborated by the two-step process is studied by AFM. The power and the duration of the first step are equal to 240 W or 420 W and 1 min, 2 min or 3 min respectively. Figure 5 shows the AFM images of the obtained pp-ANI layers.

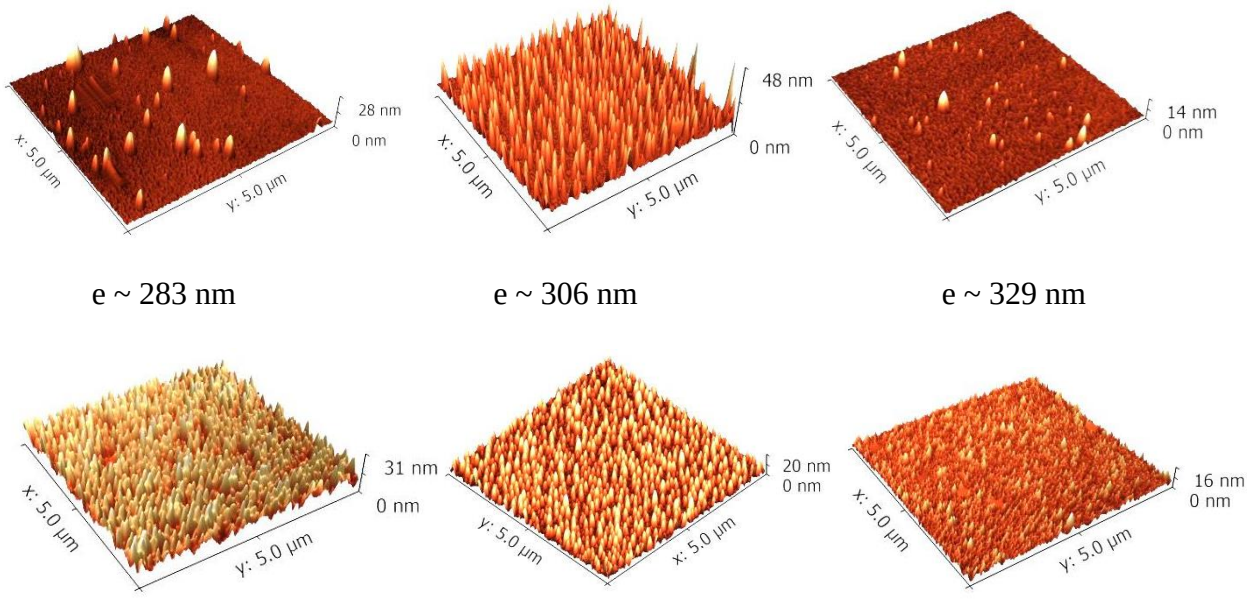

e ~ 283 nm e ~ 306 nm e ~ 329 nm

e ~ 284 nm e ~ 308 nm e ~ 332 nm

(a) (b) (c)

Figure 5. AFM images of pp-ANI surfaces obtained at 240 W (top images) or 420 W (bottom images) during a) 1 min; b) 2 min; c) 3 min. “e” corresponds to the film thickness.

These images show that nanostructures are obtained for short duration of the first step (1 or 2 min), the nanodots tending to disappear when the duration is increased.

In order to quantify the changes in morphology versus discharge power and duration, the mean square roughness (R_q) and the mean height (H) of the formed features are used. The results are presented in Figure 6.

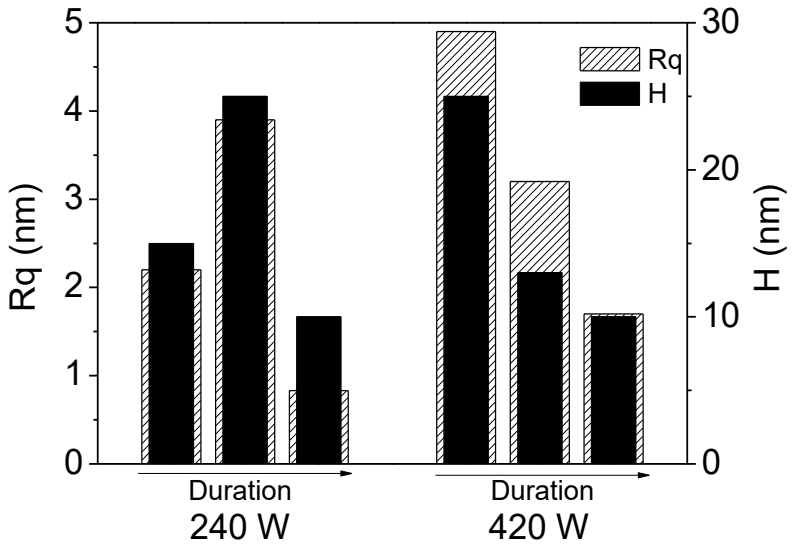

Figure 6. Mean square roughness (Rq) and height (H) of nanostructures obtained for different durations (1, 2 or 3 min) and input powers (240 W, 420 W) of the first step.

These data reflect the morphology of pp-ANI films determined by AFM. The maximum values of Rq and H are obtained for a deposition of 2 min at 240 W and of 1 min at 420 W. The lowest surface roughness and nanodot height are observed for a deposition time of 3 min regardless of the discharge power. As a reference, Rq value of a pp-ANI film elaborated in one step at 60 W for 26 min is equal to around 0.5 nm.

We assume that the surface structuring is associated with the partial dewetting of the deposited pp-ANI film [36]. The growing mechanism of the thin layer in gas phase is a continuous process of adsorption of atoms or molecules, their diffusion on the substrate, nucleation to form clusters, coalescence of the clusters and desorption [45]. All these phenomena are mostly dependent on surface energies of the substrate and of the deposited material as well as on the substrate temperature. Regarding surface energies, the dewetting is here favoured since the water contact angles (WCA) of silicon substrate and pp-ANI are quite different. WCA is lower than 5° for silicon

and around 80° for pp-ANI, depending on the elaboration conditions. Indeed, we have shown [46] that during plasma polymerization, loss of amino functional groups occurs and especially, at high powers. The dewetting process is also strongly dependent on the substrate temperature. In our previous study [42], we have shown that the dewetting can occur within a range of surface temperature that has been estimated between 40 and 50°C. In this range of temperature, the diffusion of reactive species on the substrate surface is more important compared to their adsorption. Reactive species mainly correspond to free radicals formed in the plasma phase. They are a part of the final polymer and impinge on the substrate surface where the polymer grows [47]. Therefore, plasma polymerization is a continuous wedging process. Moreover, if a thin layer is formed on the substrate, the wedging process is responsible for the accumulation of stress into the plasma layer during deposition. So, the layer that has accumulated internal stress can relax within the pre-determined range of temperature (40-50°C) and then degenerates into droplets. To summarize, the temperature plays a role in nanostructuring for both the diffusion of reactive species on the substrate surface and the relaxation of stress if a thin layer is formed. The surface heating rate is time- and power-dependent. High deposition time or discharge power lead to a too high surface temperature and a liquid-like film is obtained. No nanostructures can then be formed on the film.

Hence, fine tuning of the surface temperature should allow for the fine tuning of the morphological structure. Such a temperature tuning can be performed by changing the number of high-power steps as well as their duration. In paragraph 3.2, we present the results obtained for the three-step process.

3.1.3. Sensitivity to ammonia

Figure 7 shows the ammonia sensitivity of doped pp-ANI layers elaborated at different durations (1, 2 or 3 min) and input powers of the first step. The horizontal line represents the sensitivity of a smooth layer elaborated in one step at 60 W during 26 min, this sample is the reference. The graph shows the improvement of the gas sensitivity at the shortest first step duration regardless of the power compared to the smooth surface. Moreover, the sensitivity decreases with the rise of the power and the duration. Two factors can explain these results: the specific surface area of the nanostructured film and the chemical structure of the layer. The specific surface area, determined thanks to AFM images, is defined as the true surface area of pp-ANI layers observed on AFM images of 1 μm^2. The specific surface area (Table 1) of all the layers elaborated by the multi-step process is higher than that of layers synthesized in one step at 60 W which is 1 $\mu m^2/\mu m^2$. The best sensitivity is obtained for layers elaborated at 240 W during 1 min for the first step. We can conclude that a small increase in specific surface area significantly improves the layer sensitivity to gas. However, the specific surface area increases with power whereas ammonia sensitivity decreases. Moreover, at a given power, the sensitivity decreases with the rise of deposition time to become, in some cases, lower than that of the smooth layer. Therefore, we have also to take into account the chemical structure of the polymer through its radical density. It has been shown previously that from a first step power of 120 W or a deposition duration of 20 min, the radical concentration increases and thereby the cross-linking. In this study, the deposition durations of the first step are 1, 2 or 3 min. For these durations, the radical concentration remains constant but their total amount increases with the deposition duration since the layer thickness increases. A dense layer is then formed where the dopant as well as ammonia molecules can hardly diffuse, hence a decrease in sensitivity with the rise of input power or deposition duration.

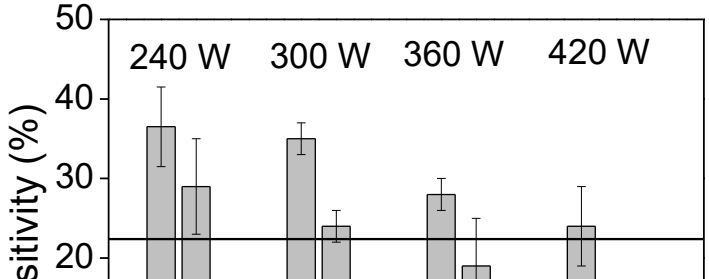

Figure 7. Ammonia sensitivity of pp-ANI layers elaborated at different durations (1, 2 or 3 min) and input powers of the first step. The horizontal line represents the sensitivity of a smooth layer elaborated in one step at 60 W during 26 min, which is the reference.

Table 1- Specific surface of pp-ANI elaborated by the two-step process at different durations and powers of the first step.

First step power (W)	240			420		
First step time (min)	1	2	3	1	2	3
Specific surface ($\mu m^2/\mu m^2$)	1.009	1.076	1.006	1.114	1.085	1.078

3.2. Three-step process

The three-step process can offer an even finer control over the surface morphology through a more precise tuning of the surface temperature by step-wise variation of the discharge power. In this process, the power of the first step is maintained at 420 W and that of the second one at 240 W. The duration of these two steps is varied from 1 min to 3 min. In the same way as in the two-step process, the power and duration of the third and last step are kept constant for all the experiments at 60 W and 26 min respectively.

3.2.1. Influence of the first step duration

The first stage of deposition must be conducted at high power (420 W) to allow the formation of the surface structure. We vary its duration from 1 min to 3 min, whereas the time and the power of the second stage remain constant at 1 min and 240 W, respectively. The AFM images of the obtained layers are presented in Figure 8.

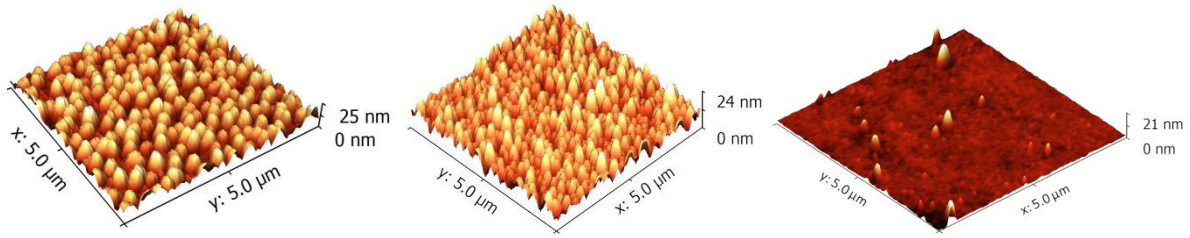

e ~ 307 nm e ~ 330 nm e ~ 355 nm

(a) (b) (c)

Figure 8. AFM images of pp-ANI films obtained at different durations of the first step: a) 1 min; b) 2 min; c) 3 min. “e” corresponds to the film thickness.

These images clearly show the formation of nanodots for short first step time. A further increase of this time leads to the evolution of the surface into relatively smooth film. The nanodots height goes from about 15 nm for 1 min of process to around 5 nm for 3 min, when at the same time, their size distribution narrows (Figure 9). Concerning the diameter of these nanostructures, it is between 300-350 nm at 1 min and 150-200 nm at 3 min. All these results prove the smoothing of the polymer surface when the first step duration increases.

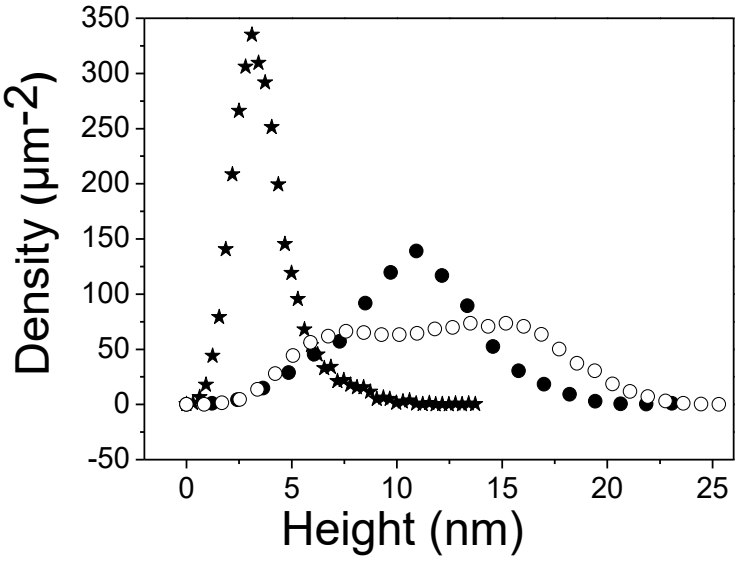

Figure 9. Height distribution of the films at different durations of the first step: (○) 1 min, (●) 2 min, (★) 3 min.

3.2.2. Influence of the second step duration

In this section, the duration of the second stage is varied from 1 to 3 min while that of the first one is maintained constant at 1 min or 2 min. The morphology of the obtained films determined by AFM is presented in Figure 10.

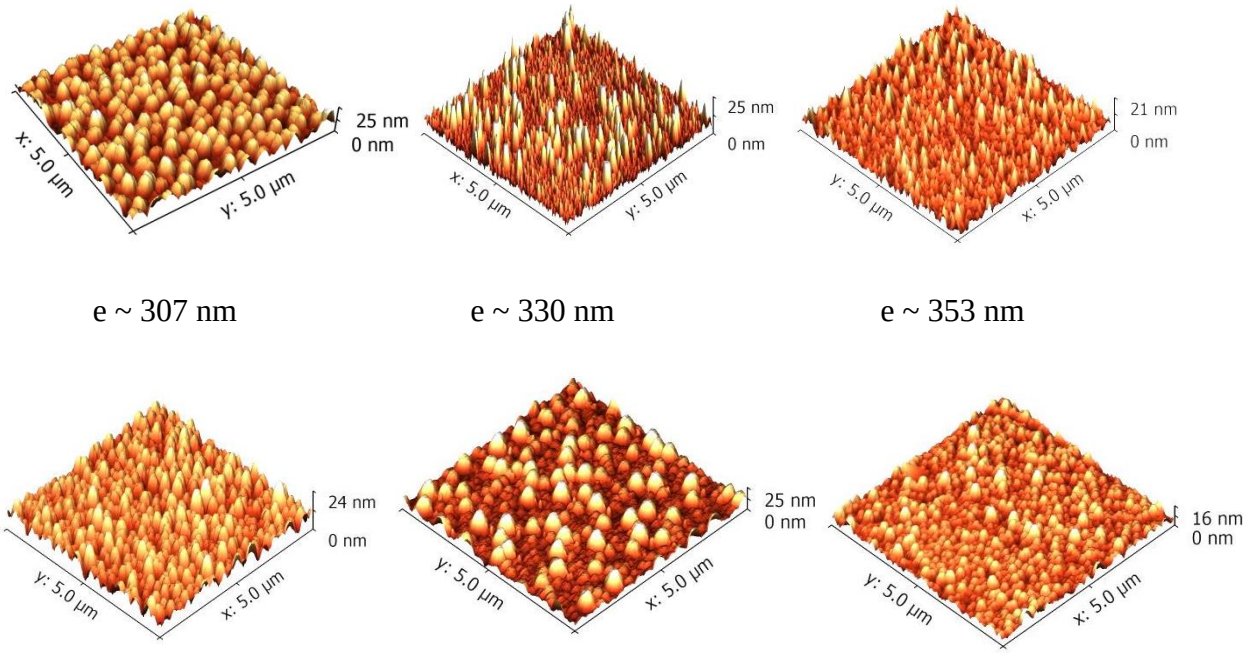

Figure 10. AFM images of pp-ANI films elaborated at a first step duration of 1 min (top images) or 2 min (bottom images) (*P* = 420 W) and at different durations of the second step: a) 1 min; b) 2 min; c) 3 min (*P* = 240 W). "e" corresponds to the film thickness.

The duration of the second step has the same influence on the surface texturing than that of the first one whatever the duration of the first step. The grains on the surface decrease in height and in diameter but also in density when the second step duration increases. Therefore, the lower the duration of the first and second steps, the higher the surface structuring is.

As mentioned above, the structuring relates to the substrate temperature variation with deposition duration and input power. In order to describe the effect of the surface temperature (T_s), it has been correlated with the values of the full width at half maximum (FWHM) of the height distribution and the root mean square roughness (R_q) of the pp-ANI surfaces (Figure 11).

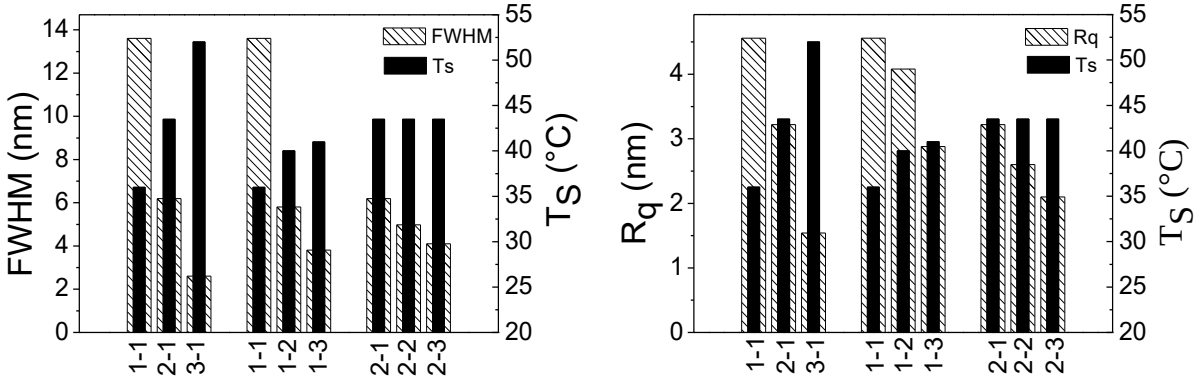

(a) (b)

Figure 11. a) Changes in FWHM with T_S; b) Changes in R_q with T_S. Numbers at the bottom stand for duration of the first and the second step respectively (min).

Figure 11 reveals a strong dependence of FWHM and R_q on substrate temperature for the first two sets. Indeed, these two parameters decrease with the rise of the surface temperature. These results confirm the effect of surface temperature through the dewetting process and the formation of a liquid-like state of the film at high deposition durations.

However, when the first step duration is equal to 2 min, Ts remains almost constant when the second step duration increases whereas FWHM and Rq decrease. We can suppose that the high energy input during the first step (420 W; 2 min) masks the energy provided by the second step (240 W; 1, 2 or 3 min). This leads to an "apparent temperature" that remains almost constant whatever the time of the second step. However, at the local scale, the energy from the second stage depends upon its duration and can contribute to the surface morphology through a more or less structured surface.

3.2.3. Sensitivity to ammonia

Figure 12 shows the ammonia sensitivity of pp-ANI layers elaborated at different durations (1 or 2 min) of the second step. The horizontal line represents the sensitivity of the reference. The graph shows the improvement of the gas sensitivity at the highest second step duration compared to the smooth surface. It can be explained by the rise of the pp-ANI specific surface from 1.004 $\mu m^2/\mu m^2$ for 1 min to 1.011 $\mu m^2/\mu m^2$ for 2 min. This result shows also the importance of the middle layer where the high amount of radicals formed in the first layer diffuse mainly in the second one without changing a lot the chemical structure of the third one elaborated at 60 W. In order to illustrate this conclusion, the sensitivity of the pp-ANI layer goes from 24 % without the middle layer (Figure 7) to 29 % with the middle layer elaborated at 240 W during 2 min (Figure 12).

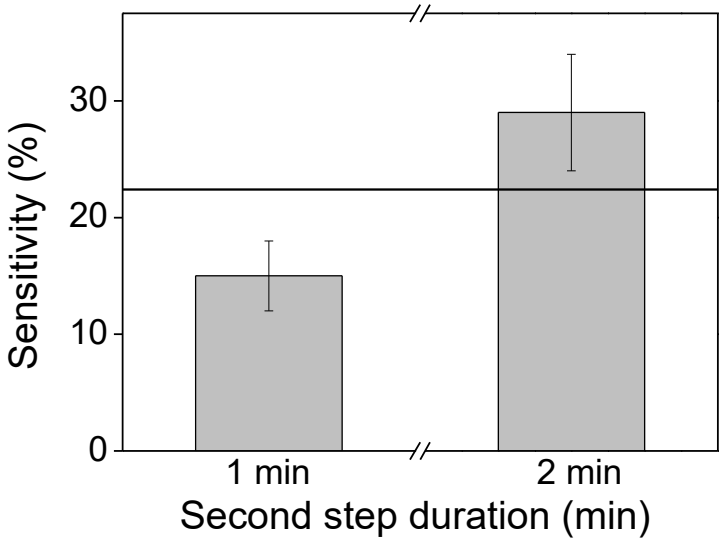

Figure 12. Ammonia sensitivity of pp-ANI layers elaborated at different durations (1 or 2 min) of the second step ($P_{first\ step}$ = 420 W, $t_{first\ step}$ = 1 min, $P_{second\ step}$ = 240 W). The horizontal line represents the sensitivity of a smooth layer elaborated in one step at 60 W during 26 min, which is the reference.

4. Conclusion

A surface clustering preserving the monomer structure takes place during plasma deposition of polyaniline with power variation. It seems to be influenced the most by the substrate temperature. With its increase, the clusters degenerate into a smooth film with low roughness and narrow height distribution. It is mandatory to proceed first with high power in order to activate the diffusion of the deposited species. However this stage should be short to limit the destruction of the formed clusters. By modulation of the surface temperature by means of time-power variation, it is possible to control the height-diameter distribution of the formed clusters as well as their density. This method is supposed to be suitable for any type of monomer since the formation of nanostructures does not depend on chemical structure of the polymer. These textured films have shown an improved sensitivity to ammonia compared to the smooth layer if elaborated at short first step power and duration in the two-step process. Moreover, the middle layer formed with the three-step process allows controlling the chemistry of all the pp-ANI film.

Acknowledgements

This work was financially supported by *La Région Pays de la Loire* through the ComPANI project.

Data availability

The raw/processed data required to reproduce these findings cannot be shared at this time due to technical or time limitations.

References

(1) Nicolas-Debarnot, D.; Poncin-Epaillard, F. *Anal. Chim. Acta* **2003**, *475*, 1–15.

(2) Kebiche, H.; Debarnot, D.; Merzouki, A.; Poncin-Epaillard, F.; Haddaoui, N. *Anal. Chim. Acta* **2012**, *737*, 64–71.

(3) Mérian, T.; Debarnot, D.; Rouessac, V.; Poncin-Epaillard, F. *Talanta* **2010**, *81*, 602–608.

(4) Gvozdenović, M. M.; Jugović, B. Z.; Stevanović, J. S.; Trišović, T. L.; Grgur, B. N. Electrochemical Polymerization of Aniline. In *Electropolymerization*; Schab-Balcerzak, E., Ed.; InTech, **2011**; pp 78–96.

(5) Chen, Y.; Kang, E. T.; Neoh, K. G. *Appl. Surf. Sci.* **2002**, *185*, 267–276.

(6) Ciric-Marjanovic, G.; Dragicevic, L.; Milojevic, M.; Mojovic, M.; Mentus, S.; Radulovic, A.; Vukovic, Z.; Stejskal, J. *J. Phys. Chem. B* **2009**, *113*, 7116–7127.

(7) Konyushenko, E. N.; Stejskal, J.; Šeděnková, I.; Trchová, M.; Sapurina, I.; Cieslar, M.; Prokeš, J. *Polym. Int.* **2006**, *55*, 31-39.

(8) Li, D.; Huang, J.; Kaner, R. B. *Acc. Chem. Res.* **2009**, *42*, 135–145.

(9) Liang, L.; Liu, J.; Windisch, C. F.; Exarhos, G. J.; Lin, Y. *Angew. Chem. Int. Ed* **2002**, *41*, 3665–3668.

(10) Liu, J.; Lin, Y.; Liang, L.; Voigt, J. A.; Huber, D. L.; Tian, Z. R.; Coker, E.; McKenzie, B.; McDermott, M. J. *Chem. a Eur. J.* **2003**, *9*, 604–611.

(11) Sutar, D. S.; Padma, N.; Aswal, D. K.; Deshpande, S. K.; Gupta, S. K.; Yakhmi, J. V. *Sensors Actuators B Chem.* **2007**, *128*, 286–292.

(12) Kavitha, B.; Kumar, K. S.; Narsimlu, N. *Indian J. Pure Appl. Phys.* **2013**, *51*, 207–209.

(13) Stejskal, J.; Sapurina, I.; Trchová, M. *Prog. Polym. Sci.* **2010**, *35*, 1420–1481.

(14) Jackowska, K.; Bieguński, A. T.; Tagowska, M. *J. Solid State Electrochem.* **2008**, *12*, 437–443.

(15) Xiong, S.; Wang, Q.; Xia, H. *Synth. Met.* **2004**, *146*, 37–42.

(16) Gao, W.; Sattayasamitsathit, S.; Orozco, J.; Wang, J. *J. Am. Chem. Soc.* **2011**, *133*, 11862–

11864.

(17) Wang, Z.; Chen, M.; Li, H. *Mater. Sci. Eng. A* **2002**, *328*, 33–38.

(18) Ahuja, T.; Kumar, D. *Sensors Actuators B Chem.* **2009**, *136*, 275–286.

(19) Zhang, D.; Wang, Y. *Mater. Sci. Eng. B* **2006**, *134*, 9–19.

(20) Cao, Y.; Mallouk, T. E. *Chem. Mater.* **2008**, *20*, 5260–5265.

(21) Tamirisa, P. A.; Liddell, K. C.; Pedrow, P. D.; Osman, M. A. *J. Appl. Polym. Sci.* **2004**, *93*, 1317–1325.

(22) Mathai, C. J.; Saravanan, S.; Anantharaman, M. R.; Venkitachalam, S.; Jayalekshmi, S. *J. Phys. D. Appl. Phys.* **2002**, *35*, 2206–2210.

(23) Wang, J.; Neoh, K. G.; Zhao, L.; Kang, E. T. *J. Colloid Interface Sci.* **2002**, *251*, 214–224.

(24) Debarnot, D.; Mérian, T.; Poncin-Epaillard, F. *Plasma Chem. Plasma Process.* **2011**, *31*, 217–231.

(25) Shepsis, L. V.; Pedrow, P. D.; Mahalingam, R.; Osman, M. A. *Thin Solid Films* **2001**, *385*, 11–21.

(26) Kumar, R.; Singh, S.; Misra, A. . K. *J. Miner. Mater. Charact. Eng.* **2010**, *9*, 997–1006.

(27) Tiwari, A.; Kumar, R.; Prabaharan, M.; Pandey, R. R.; Kumari, P.; Chaturvedi, A.; Mishra, A. K. *Polym. Adv. Technol.* **2010**, *21*, 615–620.

(28) Michelmore, A.; Martinek, P.; Sah, V.; Short, R. D.; Vasilev, K. *Plasma Process. Polym.* **2011**, *8*, 367–372.

(29) Choukourov, A.; Biederman, H.; Slavinska, D.; Hanley, L.; Grinevich, A.; Boldyryeva, H.; Mackova, A. *J. Phys. Chem. B* **2005,** *109*, 23086-23095.

(30) Hegemann, D. *Thin Solid Films* **2015**, 581, 2–6.

(31) Cicala, G.; Milella, A.; Palumbo, F.; Favia, P. *Diam. Relat. Mater.* **2003**, *12*, 2020–2025.

(32) Di Mundo, R.; Gristina, R.; Sardella, E.; Intranuovo, F.; Nardulli, M.; Milella, A.; Palumbo, F.; d'Agostino, R.; Favia, P. *Plasma Process. Polym.* **2010**, 7, 212–223.

(33) Brioude, M. M.; Laborie, M.-P.; Airoudj, A.; Haidara, H.; Roucoules, V. *Plasma Process. Polym.* **2014**, 11, 943–951.

(34) Brioude, M. M.; Laborie, M.-P.; Haidara, H.; Roucoules, V. *Plasma Process. Polym.* **2015**, 12, 1220–1230.

(35) Kato, T.; Jeong, G.-H.; Hirata, T.; Hatakeyama, R.; Tohji, K.; Motomiya, K. *Chem. Phys. Lett.* **2003**, *381*, 422–426.

(36) Meyyappan, M.; Delzeit, L.; Cassell, A.; Hash, D. *Plasma Sources Sci. Technol.* **2003**, *12*, 205–216.

(37) Astruc, D. *Inorg. Chem.* **2007**, *46*, 1884–1894.

(38) Dupuis, A. *Prog. Mater. Sci.* **2005**, *50*, 929–961.

(39) Wohlfart, E.; Fernández-Blázquez, J. P.; Knoche, E.; Bello, A.; Pérez, E.; Arzt, E.; del Campo, A. *Macromolecules* **2010**, *43*, 9908–9917.

(40) Di Mundo, R.; Troia, M.; Palumbo, F.; Trotta, M.; D'Agostino, R. *Plasma Process. Polym.* **2012**, *9*, 947–954.

(41) Gogolides, E.; Constantoudis, V.; Kokkoris, G.; Kontziampasis, D.; Tsougeni, K.; Boulousis, G.; Vlachopoulou, M.; Tserepi, A. *J. Phys. D. Appl. Phys.* **2011**, *44*, 174021.

(42) Zaitsev, A.; Poncin-Epaillard, F.; Lacoste, A.; Debarnot, D. *Plasma Process. Polym.* **2016**, *13*, 227-235.

(43) Attwood, A. L.; Murphy, D. M.; Edwards, J. L.; Egerton, T. A.; Harrison, R. W. *Res.Chem. Intermed.* **2003**, *529*, 449-465.

(44) Kassiba, A.; Bednarski, W.; Pud, A.; Errien, N.; Makowska-Janusik, M.; Laskowski, L.; Tabellout, M.; Kodjikian, S.; Fatyeyeva, K.; Ogurtsov, N.; Noskov, Y. *J. Phys. Chem. C* **2007**, *111*, 11544-11551.

(45) Venables, J. A.; Spiller, G. D. T.; Hanbücken, M. *Rep. Prog. Phys.* **1984,** *47*, 399–459.

(46) Ndiaye, A. A.; Lacoste, A.; Bès, A.; Zaitsev A.; Poncin-Epaillard F.; Debarnot, D. *Plasma Chem. Plasma Process.* **2018**, *38*, 887-902.

(47) Yasuda H. Plasma Polymerization. Academic Press, 1985.